XLVI CILAMCE
VITÓRIA - ES - BRAZIL - 2025
XLVI IBERO-LATIN AMERICAN CONGRESS ON COMPUTATIONAL METHODS IN ENGENEERING

A finite element approach for evaluation of the moment–curvature response of flexible risers

Johon L. S. Rocha[1], Gabriel B. A. de Matos[1], Marcelo S. Júnior[1], Elias S. Barroso[1], Evandro Parente Jr.[1], Antônio M. C. de Melo[1]

[1]*Laboratório de Mecânica Computacional e Visualização (LMCV), Departamento de Engenharia Estrutural e Construção Civil, Universidade Federal do Ceará*
Campus do Pici, Bloco 728, 60440-900, Ceará-Brazil
johonlenon@alu.ufc.br, gabriel.braga@alu.ufc.br, marcelomedeiros@ufc.br, elias.barroso@ufc.br, evandro@ufc.br, macario@ufc.br

Abstract. Flexible risers are critical components used in the oil and gas industry, designed to withstand high loads resulting from their self-weight, environmental actions (such as ocean currents and waves), as well as motions imposed by floating platforms. These systems are engineered to exhibit high axial tensile stiffness combined with low bending stiffness — a key characteristic for applications in dynamic environments. This work proposes a methodology to estimate the moment–curvature relationship by defining an envelope between two finite element models: one accounting for manufacturing residual pressures and another with applied axial tension. The carcass and pressure armor are modeled as equivalent orthotropic shells, the polymeric layers as isotropic shells, and the tensile armors as solid elements to capture local sliding. Contact and friction between layers are represented explicitly. The approach is applied to an experimentally tested eight-layer unbonded flexible riser. The results show that the proposed envelope accurately captures the variation in bending stiffness and the hysteresis cycles.

Keywords: Flexible riser, moment–curvature response, offshore riser, computational modeling, analytical model

1 Introduction

Flexible risers are composed of multiple structural and non-structural layers, each fulfilling a specific function. These structural elements may have their layers arranged in either bonded or unbonded configurations and, according to American Petroleum Institute [1], generally combine low bending stiffness with high axial stiffness. The metallic layers serve to withstand loads, including internal and external pressures as well as tensile forces and bending moments applied to the pipe, and are interspaced with layers of polymeric material. The internal and external polymeric sealing layers generally function to ensure the riser's tightness, preventing contact between the internal and external fluids and the metallic layers. In addition to this role, polymeric layers such as anti-wear tapes, positioned between the tensile armors, serve to reduce wear and friction, allowing the relative movement of the armors and thereby preventing the increase in bending stiffness caused by the lack of sliding between layers.

The moment–curvature relationship describes the behavior of structural elements subjected to bending; that is, it maps the set of curvatures exhibited by a given element as a function of the applied bending moments. In the specific case of unbonded flexible risers, according to Witz and Tan [2], this relationship exhibits a nonlinear and hysteretic character due to the sliding mechanisms developed by the helical armors. For small curvatures, the friction between these armors and the surrounding plastic layers results in a high initial bending stiffness, which corresponds to the sum of the contributions of all layers under the assumption that plane sections remain perpendicular to the axis. In this stage, represented by the straight-line segment OA in Fig. 1, the bending stiffness (EI_0) is dominated by the contribution of the helical armors and takes on a relatively high value.

Upon reaching a certain curvature, the friction forces between the layers are overcome, initiating the relative sliding of the helical armors from the neutral axis of the riser. In this context, it is worth noting that, according to Kraincanic and Kebadze [3], the tendons composing the armors do not slide simultaneously; instead, this phenomenon progresses smoothly until a second limiting curvature is reached, as represented by curve AB in Fig. 1. After the sliding concludes, the riser attains a new stiffness (EI_1), considerably lower than the initial one and dominated by the contribution of the cylindrical polymeric layers.

In order to analytically describe the bending behavior of flexible risers, several models have been proposed

in the literature. Feret and Bournazel [4] suggested a set of linear equations capable of representing the behavior of this type of structure under axisymmetric loading. Among the various assumptions made, one that stands out is the adoption of a geodesic path for the tensile armor tendons when sliding occurs. In addition, both a general solution and a simplified approach are proposed for solving the system of equations. Kraincanic and Kebadze [3] divided the bending process into three stages, considering the transition from the no-sliding stage to full sliding as partial sliding, and developed expressions for calculating the bending stiffness at each stage. Ramos Jr [5] proposed an analytical model capable of evaluating the structural behavior of flexible risers under a combination of axisymmetric and bending loads. Bahtui et al. [6] reported combining three different analytical models into a single formulation. The proposed model accounts for the effects of sliding, interlayer separation, and the birdcaging phenomenon. Furthermore, a switching algorithm is implemented to account for the negative contact pressure resulting from interlayer separation. Witz and Tan [2] proposed a simple model for calculating the contribution of generic helical tendons to bending stiffness before and after sliding, as well as an expression for determining the critical curvature at which the stiffness changes.

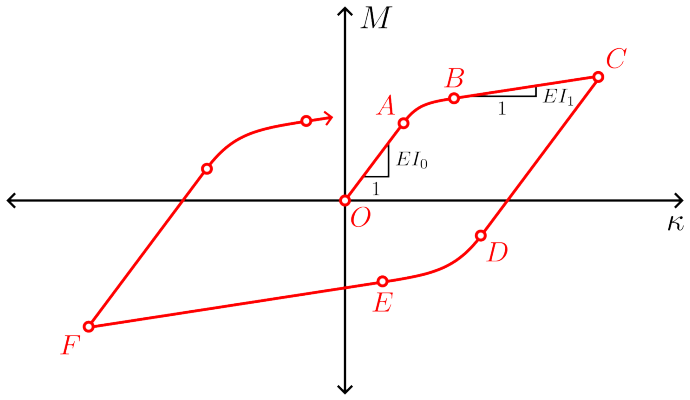


Figure 1. Typical moment–curvature relation for flexible risers.

This work aims to evaluate the moment–curvature relationship of an unbonded flexible riser reported in the literature under two limiting conditions. The first considers no external loading, accounting only for the manufacturing residual pressures. The second involves the application of axial load. For this purpose, numerical models incorporating contact and sliding between layers were developed, and an analytical formulation obtained from the literature was implemented.

2 Analytical model

Dong et al. [7] proposed a model based on the idea of partial slip from Kraincanic and Kebadze [3] and local bending from Witz and Tan [2]. Before sliding, the bending moment for a set of n tendons, with helix angle θ and at a curvature κ, can be calculated as:

$$M_1 = \frac{1}{2}nEAR^2\cos^3\theta\kappa + \frac{1}{2}n\left[EI_n\left(1+sin^2\theta\right)^2 cos\theta + EI_b\cos^7\theta + GJ\sin^2\theta cos^5\theta\right]\kappa\,, \tag{1}$$

where EA = axial stiffness of the tendon, EI_n = bending stiffness of the tendon in the normal direction, EI_b = bending stiffness of the tendon in the binormal direction and GJ = torsional stiffness of the tendon.

After sliding, the bending moment contribution is given by Equation 2, where the axial stiffness contribution is zero:

$$M_2 = \frac{1}{2}n\left[EI_n\left(1+sin^2\theta\right)^2 cos\theta + EI_b\cos^7\theta + GJ\sin^2\theta cos^5\theta\right]\kappa\,. \tag{2}$$

It is assumed here that the bending stiffness transitions abruptly from the no-slip stiffness to the full-slip stiffness once a certain curvature is reached. The boundary between the no-slip and post-slip stiffness regions is defined as the critical curvature, given by:

$$\kappa_{cr} = \frac{fq}{E\,t\,\sin\theta\,\cos^2\theta}\,, \tag{3}$$

where E = Young's modulus of the tendon, t = thickness of the tendon, f = coefficient of friction and q = contact pressure.

In the work by Witz and Tan [2], no recommendation is provided on how to obtain the contact pressure between layers. Some authors, such as Lei et al. [8] and Zhang et al. [9], estimate this pressure through numerical models. The remaining required parameters are determined from the riser's geometry and the properties of its constituent materials.

3 Finite element modeling

Numerical modeling of flexible risers for local bending behavior analysis is commonly performed using the Finite Element Method. The primary challenge of this approach lies in representing the internal carcass and pressure armors, since employing three-dimensional solid elements to model their complex geometry entails a high computational cost. In this regard, de Sousa et al. [10], when presenting a nonlinear three-dimensional finite element model to predict the response of flexible risers to loads imposed by hydraulic clamps, propose representing them as equivalent orthotropic cylindrical shells. Thus, under the criterion of preserving the original bending stiffness of the layers, the equivalent properties are expressed by:

$$h_s = \sqrt{12\frac{I_{eq}}{A}} \quad , \quad E_{sx} = \left(\frac{n_t A}{L_p h_s}\right) E \quad , \quad G_{sxy} = \left(\frac{3 n_t J}{L_p h_s^3}\right) G \quad , \tag{4}$$

where h_s, E_{sx}, and G_{sxy} are the thickness, circumferential Young's modulus, and in-plane shear modulus of the cylindrical shell, respectively; n_t is the number of tendons in the original layer; A and J are the cross-sectional area and torsional constant of a tendon; and E and G are the Young's modulus and shear modulus of the isotropic material of the original layer. Additionally, I_{eq} and L_p are the equivalent moment of inertia and the tendon pitch, defined by:

$$I_{eq} = 12 n_t \frac{I_y^2}{L_p}\frac{1-\nu^2}{h^3} \quad , \quad L_p = \frac{2\pi R}{\tan(\alpha)} \quad , \tag{5}$$

where I_y and α are the moment of inertia in the binormal direction and the lay angle of the tendons, respectively; h, R, and ν are the thickness, mean radius, and Poisson's ratio of the material of the original layer.

Regarding the modeling of tensile armors and polymeric layers, the former can be represented by three-dimensional beam elements as performed by da Cruz [11] and Badiola [12], isotropic shell elements as in the work of Lu et al. [13], or even three-dimensional solid elements, as adopted by Xiqia et al. [14], Wang and Yue [15]. However, as discussed by Pang et al. [16], the use of three-dimensional solid elements is preferable due to the effect that simplifications in other approaches have on the results. Polymeric layers, owing to their simplicity, are commonly modeled using isotropic shell elements or three-dimensional solid elements.

Another important aspect of numerical models for local bending analysis is the strategies used to simulate contact and friction between layers. In general, the use of generalized contact algorithms—that is, those considering multiple contact mechanisms among all layers throughout all loading stages—combined with the Coulomb friction model with penalty, as adopted by Lu et al. [13] and Xiqia et al. [14], is capable of adequately representing the relative sliding between helical and polymeric layers. In this regard, Dai et al. [17], presenting a reduced-scale friction test and an anisotropic model to predict friction between tensile armors and anti-wear polymeric layers of flexible risers, concluded that the decrease in the friction coefficient value during the transition from static to dynamic regime is small, so that the use of a single average coefficient, typically between 0.1 and 0.2, yields sufficiently accurate results.

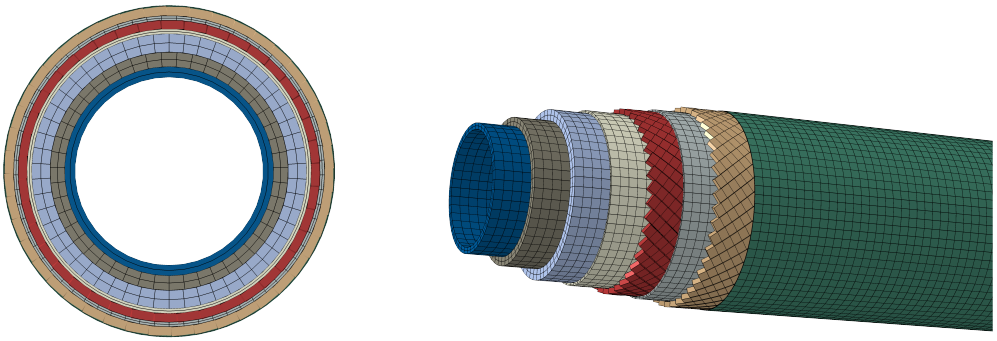
The numerical model presented in this article was developed based on the eight-layer flexible riser tested by Witz [18]. This work provides various geometric and material parameters that contribute to the creation of a representative numerical model. The details of the geometry and materials of each riser layer are listed in Table 1. In this experimental program, three mechanical properties were evaluated: tensile response, torsion, and bending of the flexible riser. These results are useful for verifying the compliance of the numerical model proposed in the present study.

Table 1. Geometric and material parameters of each layer.

Layer	ID (mm)	Thickness (mm)	E (MPa)	Density (kg/m^3)	Structural modelling
Carcass	63.2	3.50	199000	7930	Orthotropic shell
Fluid barrier	70.2	4.95	0.284	1080	Isotropic shell
Pressure armor	80.1	6.20	207000	7850	Orthotropic shell
Anti-wear layer 1	92.5	1.50	0.301	1040	Isotropic shell
Tensile armor 1	95.5	3.00	211000	7870	Solid
Anti-wear layer 2	101.5	1.50	0.301	1040	Isotropic shell
Tensile armor 2	104.5	3.00	211000	7870	Solid
Outer sheath	110.5	0.50	0.600	800	Isotropic shell

The numerical model has a length of 0.5 m, in order to establish a comparison parameter with the models analyzed by Pang et al. [16], and the layers were discretized using the element types described in Table 1. As previously noted, the interlocked carcass and pressure armor are better discretized as orthotropic shell models. The polymeric layers are typically modeled using isotropic shell elements. Finally, to accurately capture the sliding effect of the tensile armor, these were discretized with solid elements.

The complete model is thus obtained by assembling all the layers, as shown in Fig. 2, where the layers modeled as shells are represented with their respective thicknesses. In total, 44296 elements are used, of which 33700 are linear quadrilateral shell elements and 10596 are linear hexahedral solid elements with reduced integration.



(a) Cross section. (b) Overview of the numerical model.

Figure 2. Geometry of the numerical model.

For the tension model, the loading was applied through a prescribed axial displacement of 3 mm at a reference point at one end of the model. This displacement is based on the loading applied in the test by Witz [18]. At the opposite end, all degrees of freedom were constrained at a reference point. For the model with external pressure application, a pressure of 1 MPa, based on the study by Lei et al. [8], was applied to the surface of the riser's outermost layer. All degrees of freedom at both ends were constrained for this model.

Initially, a purely static analysis was performed. However, due to convergence difficulties, dynamic analyses were carried out using the explicit algorithm of the Abaqus software. With automatic time increment control, the analyses were executed with a time step of 3.5×10^{-7} s. Using the contact pressure values between the tensile armor and the polymeric layers, the equations from the analytical model of Witz and Tan [2] were applied, and an envelope for the moment–curvature relationship of the tested riser was estimated.

4 Results

The result of the tension model is compared with the first loading cycle of the experimental program by Witz [18]. Fig. 3 presents the results of the initial static analysis, the dynamic analysis using the explicit algorithm, and

the experimental data. It can be observed that the static analysis reasonably follows the dynamic analysis curve until convergence issues arise. The axial stiffness obtained from the dynamic analysis is very close to the axial stiffness measured in the experimental program at approximately 0.2% strain. In this region, the structure exhibits an almost linear response. The axial stiffness value from the experiment is on the order of 90.58 MN, while the numerical result is 97.5 MN. The portion up to 0.2% strain shows slight nonlinearity, which can be attributed to the initial accommodation of the riser layers.

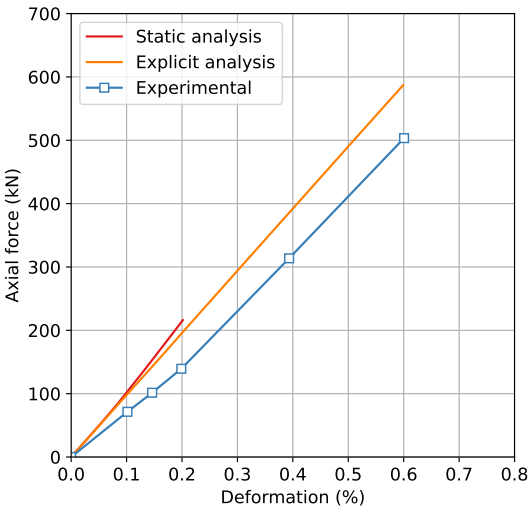


Figure 3. Axial tension vs. strain curve (Data from [18]).

Fig. 4 shows the results of the contact pressures between the outermost tensile armor and the internal anti-wear layer. The average contact pressure between these layers was 14.21 MPa, representing the highest interlayer pressure obtained in the numerical model.

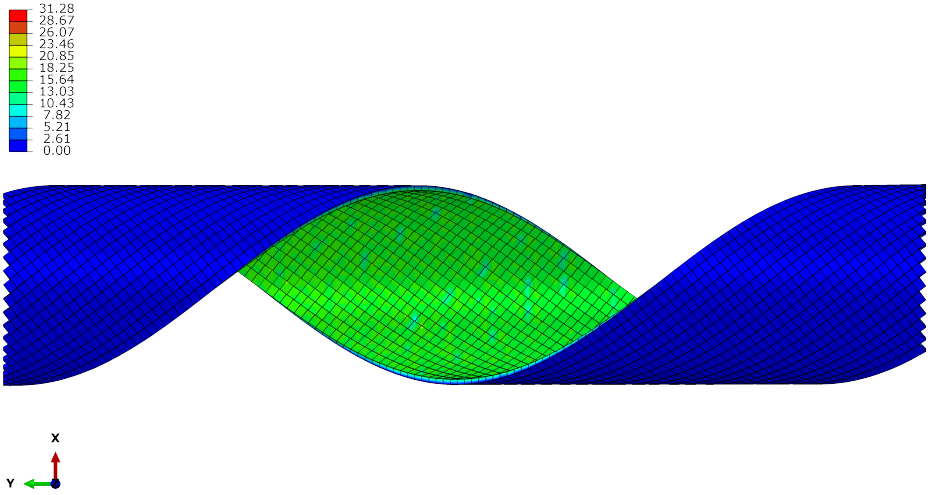


Figure 4. Contact pressure distribution on the outer tensile armor — Tension model.

For the model with external pressure application, the contact pressure result between the outer tensile armor and the internal anti-wear layer is shown in Fig. 5. The average contact pressure obtained was 1.3 MPa. This pressure is consistent with the study by Lei et al. [8], which served as a reference for this type of loading. Thus, assuming that bending loading does not introduce significant interlayer contact pressures, an envelope of the moment–curvature relationship can be obtained using the pressures of 1.3 and 14.21 MPa.

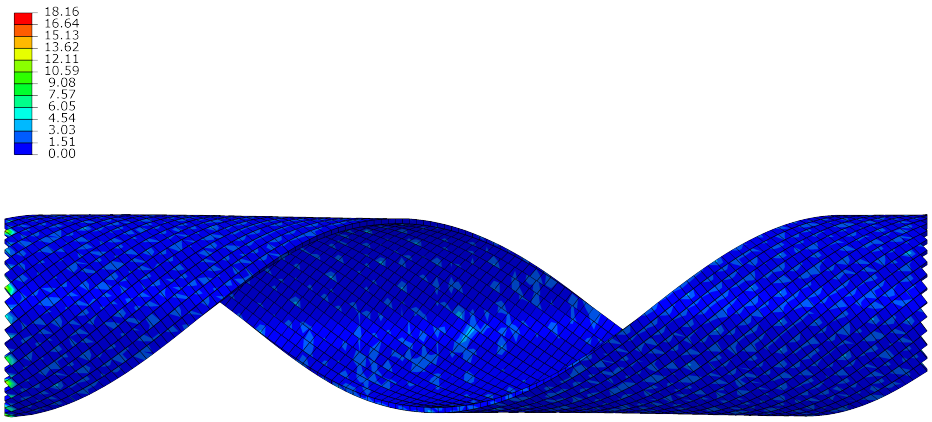
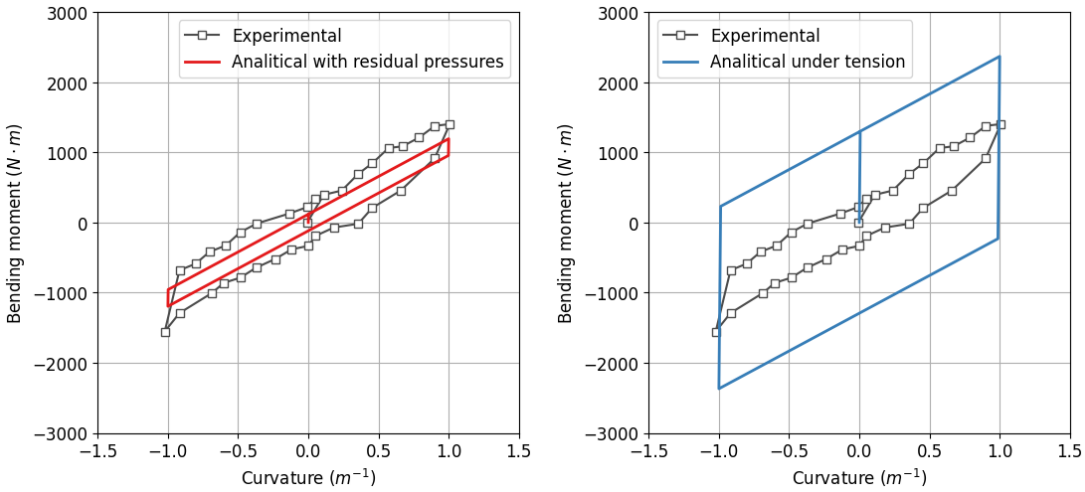


Figure 5. Contact pressure distribution on the outer tensile armor — Pressure model.

Figure 6 compares the analytical results obtained using the formulation of Dong et al. [7] for the two contact pressures derived from the numerical models, together with the experimental bending program reported by Witz [18]. For residual pressures, the numerical model shows good agreement with the experimental results in the initial loading phase. This outcome is expected, as the referenced experiment was performed without internal or external pressures, only manufacturing residual pressures, which were reproduced in the numerical model by applying a small external pressure. For the same reason, the curve corresponding to applied tension presents a substantially higher critical curvature than that observed in the experimental program. This behavior outlines a reasonable envelope of the values that such a structure may display over its service life..



(a) Structure under residual manufacturing pressures.

(b) Structure under axial tension.

Figure 6. Comparison of the analytical and experimental moment–curvature relationships.

Table 2 shows the bending stiffness and critical curvature for both cases. According to the formulation assumptions, contact pressures are not primary parameters in the stiffness calculation and thus only affect the critical curvature. The critical curvature of the model under axial tension is one order of magnitude higher than that of the model with residual pressures. This behavior results from the Poisson-induced radial contraction, which increases the interlayer contact pressure and, consequently, the overall bending resistance.

Furthermore, Table 3 presents the contribution of each layer to the total bending stiffness immediately before

Table 2. Analytical bending stiffness and critical curvatures of the analyzed models.

Model	No-slip stiffness (kNm^2)	Full-slip stiffness (kNm^2)	Critical curvature (m^{-1})
Experimental	-	1.19 / 1.01	-
Under pressure	221.66	1.08	0.00583
Under tension	221.66	1.08	0.00053

and after slip. Prior to slip, the tensile layer predominantly governs the bending stiffness, accounting for approximately 99.65% of the total. Conversely, after slip, the overall stiffness decreases, and the polymeric layers become the main contributors. The carcass and pressure armour are two helical layers with lay angles close to 90°, thus their axial contribution to the bending stiffness is nearly negligible. In this case, local bending governs their stiffness contribution, which is minimal, accounting for only 3.18% after slip. As the key determinants of the bending stiffness after slip, it is crucial to account for the elastic modulus of the polymeric layers when estimating these values in practical applications.

Table 3. Contribution of each layer to the total stiffness immediately before and after slip.

Layer	No-slip stiffness (kNm^2)	Contribution	Full-slip stiffness (kNm^2)	Contribution
Carcass	0.009	0.00%	0.009	0.87%
Pressure Sheath	0.23	0.10%	0.23	21.61%
Pressure Armour	0.24	0.01%	0.25	2.31%
Inner Anti-wear layer	0.15	0.07%	0.15	13.69%
Inner tensile layer	95.34	43.01%	0.15	13.58%
Outer Anti-wear layer	0.19	0.09%	0.19	18.01%
Outer tensile layer	125.55	56.64%	0.16	14.94%
Outer sheath	0.16	0.07%	0.16	14.98%

5 Conclusions

This work proposed a methodology for determining the moment–curvature relationship of unbonded flexible risers, based on constructing an envelope derived from two finite element models: one considering manufacturing residual stresses and the other with applied axial tension. The modeling adopted equivalent representations for the metallic and polymeric layers, as well as solid elements for the tensile armors, allowing a more accurate capture of the relative sliding effect between layers.

The comparison of numerical results with experimental data from the literature demonstrated that the proposed strategy is capable of satisfactorily reproducing the variation in bending stiffness and the characteristic hysteretic behavior of these systems. It was observed that the explicit consideration of contact and friction between layers is essential for a realistic representation of the phenomenon, especially for extracting contact pressures.

The approach presented herein enhances the understanding of the bending behavior of flexible risers and can serve as a practical tool for their design and structural assessment. This study is ongoing, and future work may extend the model to incorporate the effects of pure bending, combined loading, temperature variations, and material degradation over the service life of the structure.

Acknowledgements. This research was supported by PETROBRAS and the Conselho Nacional de Desenvolvimento Científico e Tecnológico (CNPq). The authors gratefully acknowledge the financial assistance provided by these institutions.

Authorship statement. The authors hereby confirm that they are the sole liable persons responsible for the authorship of this work, and that all material that has been herein included as part of the present paper is either the

property (and authorship) of the authors, or has the permission of the owners to be included here.

References

[1] American Petroleum Institute. Api recommended practice 17b: Recommended practice for flexible pipe. Recommended Practice API RP 17B, American Petroleum Institute, Washington, D.C., 2008.
[2] J. A. Witz and Z. Tan. On the flexural structural behaviour of flexible pipes, umbilicals and marine cables. *Marine Structures*, vol. 5, pp. 229–249, 1992.
[3] I. Kraincanic and E. Kebadze. Slip initiation and progression in helical armouring layers of unbonded flexible pipes and its effect on pipe bending behaviour, 2001.
[4] J. J. Feret and C. L. Bournazel. Calculation of stresses and slip in structural layers of unbonded flexible pipes. Technical report, 1987.
[5] R. Ramos Jr. Modelos analíticos no estudo do comportamento estrutural de tubos flexíveis e cabos umbilicais, 2001.
[6] A. Bahtui, H. Bahai, and G. Alfano. Numerical and analytical modeling of unbonded flexible risers. *Journal of Offshore Mechanics and Arctic Engineering*, vol. 131, pp. 1–13, 2009.
[7] L. Dong, Y. Huang, Q. Zhang, and G. Liu. An analytical model to predict the bending behavior of unbonded flexible pipes. *Journal of Ship Research*, vol. 57, pp. 171–177, 2013.
[8] Q. Lei, C. Chen, and X. Zhu. Analysis of the bending performance of unbonded flexible risers. *Ships and Offshore Structures*, 2024.
[9] X. Zhang, S. Wang, W. Ma, L. Su, and Y. Yang. Study on the influence of bending curvature on the bending characteristics of unbonded flexible pipes. *Ocean Engineering*, vol. 281, 2023.
[10] de J. R. Sousa, C. Magluta, N. Roitman, G. B. Ellwanger, E. C. Lima, and A. Papaleo. On the response of flexible risers to loads imposed by hydraulic collars. *Applied Ocean Research*, vol. 31, pp. 157–170, 2009.
[11] da F. T. L. Cruz. Análise estrutural de linhas flexíveis pelo método dos elementos finitos, 1996.
[12] G. V. Badiola. Análise local de duto flexível pelo método dos elementos finitos, 2016.
[13] H. Lu, M. A. Vaz, and M. Caire. A finite element model for unbonded flexible pipe under combined axisymmetric and bending loads. *Marine Structures*, vol. 74, pp. 102826, 2020.
[14] C. Xiqia, F. Shixiao, G. Yun, and D. Xiaying. A finite element analysis for unbonded flexible risers under bending loads. *Ocean Systems Engineering*, vol. 5, pp. 77–89, 2015.
[15] L. Wang and Q. Yue. A full layered numerical model for predicting hysteretic behavior of unbonded flexible pipes considering initial contact pressure. *Applied Ocean Research*, vol. 111, pp. 102626, 2021.
[16] G. Pang, C. Chen, Y. Shen, and F. Liu. Comparison between different finite element analyses of unbonded flexible pipe via different modeling patterns. *Journal of Shanghai Jiaotong University (Science)*, vol. 24, pp. 357–363, 2019.
[17] T. Dai, S. Sævik, and N. Ye. An anisotropic friction model in non-bonded flexible risers. *Marine Structures*, vol. 59, pp. 423–443, 2018.
[18] J. A. Witz. A case study in the cross-section analysis of flexible risers. Technical report, 1996.